

Air-Ground Spatial Crowdsourcing with UAV Carriers by Geometric Graph Convolutional Multi-Agent Deep Reinforcement Learning

Yu Wang

*School of Computer Science
Beijing Institute of Technology
Beijing, China
3120201075@bit.edu.cn*

Jingfei Wu

*School of Computer Science
Beijing Institute of Technology
Beijing, China
jingfeiwu@bit.edu.cn*

Xingyuan Hua

*School of Computer Science
Beijing Institute of Technology
Beijing, China
1120200695@bit.edu.cn*

Chi Harold Liu

*School of Computer Science
Beijing Institute of Technology
Beijing, China
chiliu@bit.edu.cn*

Guozheng Li

*School of Computer Science
Beijing Institute of Technology
Beijing, China
guozheng.li@bit.edu.cn*

Jianxin Zhao

*School of Computer Science
Beijing Institute of Technology
Beijing, China
jianxin.zhao@bit.edu.cn*

Ye Yuan

*School of Computer Science
Beijing Institute of Technology
Beijing, China
yuan-ye@bit.edu.cn*

Guoren Wang

*School of Computer Science
Beijing Institute of Technology
Beijing, China
wanggr@bit.edu.cn*

Abstract—Spatial Crowdsourcing (SC) has been proved as an effective paradigm for data acquisition in urban environments. Apart from using human participant, with the rapid development of unmanned vehicles (UVs) technologies, unmanned aerial or ground vehicles (UAVs, UGVs) are equipped with various high-precision sensors, enabling them to become new types of data collectors. However, UGVs' operational range is constrained by the road network, and UAVs are limited by power supply, it is thus natural to use UGVs and UAVs together as a coalition, and more precisely, UGVs behave as the UAV carriers for range extensions to achieve complicated air-ground SC tasks. In this paper, we propose a novel communication-based multi-agent deep reinforcement learning method called “GARL”, which consists of a multi-center attention-based graph convolutional network (GCN) to accurately extract UGV specific features from UGV stop network called “MC-GCN”, and a novel GNN-based communication mechanism called “E-Comm” to make the cooperation among UGVs adaptive to constant changing of geometric shapes formed by UGVs. Extensive simulation results on two campuses of KAIST and UCLA campuses show that GARL consistently outperforms eight other baselines in terms of overall efficiency.

Index Terms—Spatial crowdsourcing, multi-agent reinforcement learning, graph neural network

I. INTRODUCTION

Spatial crowdsourcing (SC [1]–[3]) is an attractive paradigm that assigns a particular spatial-temporal task to a collective group of workers (normally human participants), which has many applications in ride hailing services [4], road condition monitoring [5], [6], etc. To achieve higher flexibility and lower latency, instead of using human participants, unmanned vehicles (UVs) including unmanned aerial vehicles (UAVs) and unmanned ground vehicles (UGVs) have shown great potentials to complete SC tasks, since they are equipped with high-speed data receivers like WiFi/5G to enable sensory data

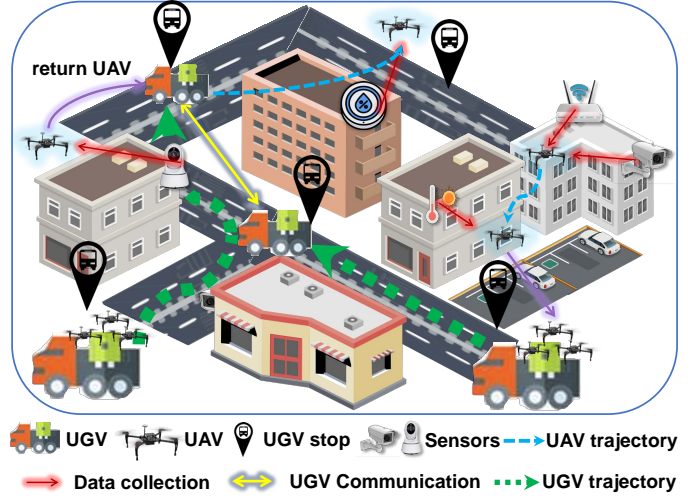


Fig. 1. Overall scenario for air-ground SC with UAV carriers.

collection and sharing in urban environment. However, since UGVs cannot reach high-up areas and UAVs are usually associated with inadequate operational range due to limited power supply, it is challenging to simply utilize one type of UVs only. Therefore, it is promising to use UGVs as “carriers” and allow UAVs to land on top of them as a *coalition* to achieve data collection services, which helps overcome their individual constraints and thus improving overall task efficiency. As shown in Fig. I, several UGV stops are located along the roads, and UAVs are loaded. UGVs also provide battery charging services for UAVs, decide which stop to go next and when to release the UAVs to fly over the workzone to collect data from a variety of deployed sensors like CCTV cameras and gas alarms. To the best of our knowledge, we are one of the first to consider air-ground SC with UAV carriers.

In an air-ground SC task with UAV carriers, key challenges are, first, rapid and unpredictable changes of the sensory data to be collected may cause difficulties for UAVs-UGV coalitions to have an overall understanding on the entire environment conditions in real-time. Along the direction of spatial modeling, existing research on graph neural networks (GNN) related methods [7], [8] can capture the features of UGV stops as graph nodes, which is constructed using road connectivity. However, in practice, the entire workzone can be really large, even if not, it is also impossible for one single UGV to know the entire graph since it has partial observations of the environment, which may in turn be resulted in overlapping/missed visits to certain sensors. Therefore, it is natural to use communication-based multi-agent deep reinforcement learning (MADRL) as the start point of the design to control UGVs/UAVs, and along this direction, many efforts have been paid. To enhance communication among agents, GAM [9] and IC3Net [10] improved the performance in cooperative scenarios by designing specific communication mechanism. However, information sharing among UGVs may be significantly influenced by practical underlying network conditions, such as communications infrastructures, network workload and obstacles to prevent signal propagation. CommNet [11] and ToM2C [12] cannot adapt to the constant changing of geometric shapes formed by UGVs, such as translation and rotation. However this kind of changes is important when the data distribution is not uniform among sensors. Hence, existing solutions lack an efficient communication mechanism for UAVs-UGV trajectory planning, which can efficiently exchange messages among UGVs, and be sensitive to geometric changes simultaneously.

To this end, in this paper, we propose a novel MADRL model called “GARL”, which extracts UGV specific features from the stop network based on an attention module, and supports efficient geometry-aware message exchange among UGVs, using IPPO [13] as the start point of the design. Our contribution is three-fold:

- We propose a novel multi-center attention-based graph convolutional network called “MC-GCN” to extract UGV specific features of stop network from their own observations of the environment.
- We propose a geometry-aware communication mechanism called “E-Comm”, which well adapts to constant changing of geometric shapes formed by UGVs including transformation and rotation.
- We perform extensive experiments on two campuses: KAIST (South Korea) and UCLA (USA). We find the most appropriate hyperparameters, and conduct ablation study, visualize the UGV/UAV trajectory, and show performance comparisons with eight baselines. Results confirm that “GARL” outperforms all others in term of overall efficiency.

The remainder of this paper is organized as follows. First, we review related activities in Section II. Then, we present the system model in Section III and give problem definition

TABLE I
IMPORTANT NOTATIONS USED IN THE PAPER.

Notation	Explanation
t, T	Time index and task duration.
\mathcal{U}, u, U	UGV set, index and total number of UGVs.
\mathcal{V}, v, V	UGV set, index and total number of UAVs.
V'	The number of UAVs on each UGV.
$\Delta d_t^{v,p}$	Data collected by a UAV v from sensor p during timeslot $[t, t + 1]$.
d_t^p	Remaining amount of data of sensor p at t .
$\lambda, \psi, \xi, \zeta, \beta$	Efficiency, data collection ratio, fairness, cooperation factor and energy consumption ratio.
\mathbf{x}_t^b	UGV stop vector of node b at t .
\mathbf{x}_t^u	UGV u ’s position at t .
\mathbf{s}_t	State at t .
$\mathbf{o}_t^u, \mathbf{o}_t^v$	Observation of UGV u and UAV v at t .
$\mathbf{a}_t^u, \mathbf{a}_t^v$	Action of UGV u and UAV v at t .

and formulation in Section IV. Next, we present our proposed method GARL in Section V. Experimental results are provided in Section VI and we conclude the paper in Section VII. We list the important notations in Table I.

II. RELATED WORK AND PRELIMINARIES

A. Spatial Crowdsourcing (SC)

With the development of high-speed mobile Internet and the increasing popularity of smart devices, people can easily get access to online services and engage in spatial-temporal cooperative tasks. A new framework, namely spatial crowdsourcing [14] is proposed to support these real-world activities. In SC, many existing solutions are proposed. For example, Ni *et al.* in [15] considered task dependencies, where one task can be assigned only if its dependent tasks have been dispatched. Based on this constraint, they proposed greedy and game-theoretic approaches. Cheng *et al.* in [16] considered worker cooperations, and they proposed a Cross Online Matching algorithm (COM), making a platform to borrow available workers from other platforms for finishing requests from users [2]. Besides, they also proposed two algorithms, including deterministic cross online matching and randomized cross online matching for COM. Given that many methods only focus on static offline scenarios, Zhao *et al.* in [17] predicted the trajectories of workers and distributions of future tasks in their proposed solutions. They paid attention to both current and future workers or tasks that enter the system dynamically. In the consideration of data privacy issues, To *et al.* in [18] proposed a Geo-Indistinguishable privacy mechanism to protect the location privacy of both workers and tasks, and they further applied a probability-based algorithm to assign tasks to workers in an online manner. In order to minimize maximum task assignment delay, Chen *et al.* in [1] proposed an efficient space embedding-based online random algorithm which gets results with at most $O(\log n)$ expected times of delay compared with other baselines in their paper.

In SC with UVs, Zhou *et al.* investigated joint optimization of route planning and task assignment problem for the sake of energy efficiency in UAV-aided SC systems [19].

Liu *et al.* developed a distributed DRL-based framework to achieve energy-efficient multi-UAV navigation, ensuring long-term communication coverage [20]. Wang *et al.* proposed FD-MAPPO (Cubic Map) [21] to enable humans to work collaboratively with UAVs to achieve data collection tasks based on a fully decentralized MADRL framework. IADRL [22] considered to use a coalition of a UGV and a UAV to complete certain tasks by combining imitation learning with DRL. However, the tight binding between one single UGV and one UAV is not optimal.

B. Graph Neural Network (GNN)

GNN methods operate on graph structured data, learning graph representation through node and edge features. Message passing scheme is the key part of these models, determining how a node aggregates information from their neighborhood in a graph. Graph convolutional networks (GCNs [7]) are the de facto method for graph processing and many related methods have been proposed to extract locally connected features from graphs [23], [24], and widely used in many applications, such as social networks [25], molecule structure modeling [26] and traffic prediction [27]. GCN is built by interleaving vertex-wise operations, implemented via a single fully-connected layer, with a communication step exploiting the Laplacian matrix of the graph. In practice, a single GCN layer provides a weighted combination of information across neighbors, representing a localized 1-hop exchange of information. A generic GCN layer can be described as:

$$\mathbf{X}^{(l+1)} = \sigma(\mathbf{L}\mathbf{X}^{(l)}\mathbf{W}), \quad (1a)$$

$$\mathbf{L} = \tilde{\mathbf{D}}^{-\frac{1}{2}}\tilde{\mathbf{A}}\tilde{\mathbf{D}}^{-\frac{1}{2}}, \quad (1b)$$

where $\tilde{\mathbf{A}} = \mathbf{A} + \mathbf{I}_N$ is the adjacent matrix with self-connection; \mathbf{L} is the Laplace matrix and $\tilde{\mathbf{D}}$ is a diagonal matrix where $\tilde{\mathbf{D}}_{ii} = \sum_j \tilde{\mathbf{A}}_{ij}$; $\mathbf{X}^{(l)}$ is the node feature matrix on l -th GCN layer and \mathbf{W} is a learnable weight matrix.

Message passing neural network (MPNN) framework [28] concludes the message passing schemes of existing neural network models for graph structured data. It operates in message passing phase and readout phase, defined as:

$$\mathbf{m}_v^{(l+1)} = \sum_{u \in \mathcal{N}(v)} M^{(l)}(\mathbf{X}_v^{(l)}, \mathbf{X}_u^{(l)}, \mathbf{e}_{vu}), \quad (2a)$$

$$\mathbf{X}_v^{(l+1)} = U^{(l)}(\mathbf{X}_v^{(l)}, \mathbf{m}_v^{(l+1)}), \quad (2b)$$

where M is the message aggregation function and U is the vertex update function; $\mathbf{m}_v^{(l)}$ is the message aggregated from the neighbors of node v ; $\mathbf{X}_v^{(l)}, \mathbf{X}_u^{(l)}$ is the feature of node v and u on the l -th layer and \mathbf{e}_{vu} is the feature vector of the edge between node v and u .

C. Multi-Agent Deep Reinforcement Learning (MADRL)

In cooperative multi-agent tasks, a decentralized partially observable Markov decision process (Dec-POMDP) [29] is used to describe partially observable environment. A Dec-POMDP is formally defined as a tuple $\langle \mathcal{U}, \mathcal{S}, \mathcal{A}, \text{Pr}, R, \mathcal{O}, \rho, \rho_0, \gamma \rangle$, where $\mathcal{U}, \mathcal{S}, \mathcal{A}$ and \mathcal{O} are the

set of agents, states, actions and observations. The initial state s_0 is drawn from distribution ρ_0 . During timeslot $[t, t+1]$, each agent $u \in \mathcal{U}$ obtains its observation $\mathbf{o}_t^u \in \mathcal{O}$, and then chooses its action \mathbf{a}_t^u based on local observation following its policy. After all agents taking the joint actions $\{\mathbf{a}_t^u\}_{u=1}^U$, the next state s_{t+1} is drawn from transition probability kernel $\text{Pr}(s_{t+1}|s_t, \{\mathbf{a}_t^u\}_{u=1}^U)$. Then, each agent u receives a individual reward $r_t^u = R(s_t, \{\mathbf{a}_t^u\}_{u=1}^U, u)$ from the environment. The aim is to maximize the discounted accumulative reward $J(\theta) = \mathbb{E}[\sum_{t=0}^{\infty} \gamma^t \sum_{u=1}^U r_t^u]$, where $\gamma \in [0, 1)$ is the discount factor.

Centralized and decentralized learning are two general frameworks in MADRL algorithms. To mitigate the instability in decentralized methods, centralized training and decentralized execution (CTDE) framework is applied [30]–[32]. However, these models still lack of ability in message exchanges among agents, especially in partially observable and stochastic environment. Many previous works have specially designed communication mechanisms. For example, TarMAC [33] used attention mechanism to learn what to send to other agents and whom to communicate with. ToM2C [12] was able to predict other agents' observation and intention to achieve efficient cooperation.

Both IPPO [13] and MAPPO [34] show competitive performance in cooperative tasks. IPPO learns independently in a fully decentralized manner while MAPPO estimates decentralized actor and centralized critic based on global state. Despite of the different frameworks, IPPO and MAPPO have similar objective functions in general, which are defined as:

$$L^{CLIP+VF+H}(\theta^u) = \mathbb{E}_t [L_t^{CLIP}(\theta^u) - c_1 L_t^{VF}(\theta^u) + c_2 H(\pi_{\theta^u})], \quad (3a)$$

$$L_t^{CLIP}(\theta^u) = \min \left(\frac{\pi_{\theta^u}(\mathbf{a}_t^u | \mathbf{h}_t^u)}{\pi_{\theta_{old}^u}(\mathbf{a}_t^u | \mathbf{h}_t^u)} A_t^u, \right. \\ \left. \text{clip} \left(\frac{\pi_{\theta^u}(\mathbf{a}_t^u | \mathbf{h}_t^u)}{\pi_{\theta_{old}^u}(\mathbf{a}_t^u | \mathbf{h}_t^u)}, 1 - \epsilon_1, 1 + \epsilon_1 \right) A_t^u \right), \quad (3b)$$

$$L_t^{VF}(\theta^u) = \max((V_{\theta^u}(\mathbf{h}_t^u) - \hat{R}_t^u)^2, (\text{clip}(V_{\theta^u}(\mathbf{h}_t^u), \\ V_{\theta_{old}^u}(\mathbf{h}_t^u) - \epsilon_2, V_{\theta_{old}^u}(\mathbf{h}_t^u) + \epsilon_2) - \hat{R}_t^u)^2), \quad (3c)$$

where $H(\pi_{\theta^u})$ denotes the entropy of policy π_{θ^u} ; c_1, c_2, ϵ_1 and ϵ_2 are constants; \mathbf{h}_t^u is the feature extracted from observation \mathbf{o}_t^u ; A_t^u is calculated via the Generalized Advantage Estimation (GAE) approach [35]; \hat{R}_t^u is the discounted reward.

III. SYSTEM MODEL

In our considered air-ground SC tasks with UAV carriers, let $\mathcal{U} \triangleq \{1, \dots, u, \dots, U\}$ and $\mathcal{V} \triangleq \{1, \dots, v, \dots, V\}$ denote UGVs and UAVs in the target workzone, respectively. Each UAV v is associated with limited initial fully-charged battery supply e_0^v . UAVs which are loaded on a UGV u are denoted as $\mathcal{V}^u \triangleq \{v | v \in \mathcal{V}, v \text{ is carried by } u\}$, where UGV u can replenish the battery of carried UAVs in \mathcal{V}^u if needed. Let V' denote the number of UAVs carried by each UGV. In a task, UGVs and UAVs cooperate to collect data from sensors

$\mathcal{P} \triangleq \{1, \dots, p, \dots, P\}$, which distribute around buildings in the target workzone. Initially, a sensor p contains $d_0^p, \forall p \in \mathcal{P}$ unit data to be collected by UAVs. Due to the limitation of the flight height and prohibited areas of UAVs by regional regulations or rules, for ease of exposition, we regard all the buildings as obstacles that UAVs cannot fly over. UGVs travel along the stop network in the target workzone, which can be abstracted into a graph called “stop graph” denoted as $\mathcal{G} = \{\mathcal{B}, \mathcal{E}\}$. Operations to construct a UGV stop graph are as follows: first, virtual UGV stop nodes $\mathcal{B} \triangleq \{1, \dots, b, \dots, B\}$ are set at regular intervals along the roads, and then the edges \mathcal{E} in \mathcal{G} are connected according to the connectivity of these virtual nodes in practice.

Without loss of generality, we consider a time-slotted system, dividing the task duration into T timeslots. In each timeslot $[t, t+1)$, each UGV u first decides whether to *release* UAVs in \mathcal{V}^u to collect data in the surrounding area or not. If a UGV u decides to do so, it flies the UAVs and then wait in its position $\mathbf{x}_t^u = (x_t^u, y_t^u)$ for a specified period t^{rls} ; otherwise, a UGV u chooses the next stop and moves over. During each timeslot, a UGV u moves a certain distance $\delta_t^u \leq \delta_{\max}^u$, and each released UAV v moves a certain distance $\delta_t^v = \sqrt{(x_{t+1}^v - x_t^v)^2 + (y_{t+1}^v - y_t^v)^2} \leq \delta_{\max}^v$ at any angle, where $\delta_{\max}^u, \delta_{\max}^v$ are the maximum distance a UGV/UAV can travel given the fixed duration of a timeslot, and $\mathbf{x}_t^v = (x_t^v, y_t^v)$ is the position of a UAV v at the beginning of this timeslot. Each UAV v will consume $\eta \delta_t^v$ unit energy for movement, where η is a weight. The released UAVs will return to the designated UGV as UAV carrier after t^{rls} timeslots and fully charged to its initial energy level e_0^v , or before t^{rls} timeslots if it runs out of battery.

At each timeslot $[t, t+1)$, if a sensor p is within the sensing range of a UAV v , the latter collects $\Delta d_t^{v,p} = \min(\Delta d^v, d_t^p)$ unit data, where Δd^v denotes the maximum amount of data each UAV v can collect from a sensor during each timeslot, and d_t^p denotes the remaining amount of data at sensor p at t .

IV. PROBLEM DEFINITION AND FORMULATION

A. Problem Definition

In air-ground collaborative SC tasks, UGVs and UAVs cooperate to collect data from deployed sensors within a sensing range, to achieve the following goals. First is to maximize the total amount of collected data in the workzone, defined as data collection ratio ψ :

$$\psi = 1 - \frac{\sum_p d_T^p}{\sum_p d_0^p}, \quad (4)$$

where $\sum_p d_0^p$ represents the initial data to be collected of all sensors in the target workzone, and $\sum_p d_T^p$ denotes the remaining data which UAVs fail to collect at the end.

Second is to try to collect data as evenly as possible among all sensors, defined as fairness ξ by using Jain’s fairness

index [36] to measure the geographically exploration range of UGVs and UAVs, as:

$$\xi = \frac{\left(\sum_p (d_0^p - d_T^p) / d_0^p \right)^2}{P \sum_p \left((d_0^p - d_T^p) / d_0^p \right)^2 + \epsilon}, \quad (5)$$

where ϵ is a small constant. Higher fairness indicates higher geographical coverage.

Third is to maximize the degree of UAVs-UGV air-ground collaboration since it is highly expected that UAVs can successfully collect sensory data every time it is released by its carrier UGV, defined as cooperation factor ζ :

$$\zeta = \frac{\sum_v \#_v^{\text{eff-rls}}}{\sum_v \#_v^{\text{rls}}}, \quad (6)$$

where $\#_v^{\text{rls}}$ denotes the total number of UAV v is released in the task duration, $\#_v^{\text{eff-rls}}$ counts the number of times a UAV v is released and actually collect data during this flight.

Fourth is to minimize the energy consumption of all UAVs due to constant movement, defined as energy consumption ratio β :

$$\beta = \frac{\sum_{v,t} \eta \delta_t^v}{\sum_v e_0^v + \sum_{v,t} \Delta e_t^v}, \quad (7)$$

where $\sum_{v,t} \Delta e_t^v$ denotes the overall charged energy for all UAVs.

Our goal is to maximize data collection ratio ψ , fairness ξ , cooperation factor ζ simultaneously, while minimizing energy consumption ratio β , which is achieved by integrating these four metrics into one single performance metric called “efficiency” λ :

$$\lambda = \frac{\psi \cdot \xi \cdot \zeta}{\beta}. \quad (8)$$

B. Problem Formulation

The state $\mathbf{s}_t \in \mathcal{S}$ of an air-ground SC task with UAV carriers contains four aspects. First is the information about the UGV stops and buildings as obstacles in the target workzone. Here we use a vector \mathbf{x}_t^b to describe a UGV stop node b in stop graph \mathcal{G} , as:

$$\mathbf{x}_t^b = [x^b, y^b, d_t^b]^\top, \forall b \in \mathcal{B}, \quad (9)$$

where (x^b, y^b) denotes the position of stop node b , and d_t^b represents the data quantity that can be collected by UAVs released by UGV in the position of stop node b at t . Second is the current position $\mathbf{x}_t^u = (x_t^u, y_t^u)$ of each UGV u . Third is the current position $\mathbf{x}_t^v = (x_t^v, y_t^v)$ of each UAV v . Finally is the position $\mathbf{x}_p = (x_p, y_p)$ and the amount of remaining data d_t^p to be collected from each sensor p .

Each UGV u has its own observation \mathbf{o}_t^u , which contains two tensors. The first tensor $\hat{\mathbf{X}}_t^{\mathcal{B},u}$ records the observation of stop nodes, as:

$$\hat{\mathbf{X}}_t^{\mathcal{B},u} = [\hat{\mathbf{x}}_t^{1,u}, \dots, \hat{\mathbf{x}}_t^{b,u}, \dots, \hat{\mathbf{x}}_t^{B,u}]^\top, \quad (10a)$$

$$\hat{\mathbf{x}}_t^{b,u} = [x^b, y^b, d_t^b]^\top, \quad (10b)$$

where $\hat{\mathbf{x}}_t^b$ is a masked vector of \mathbf{x}_t^b . Specifically, given a stop node b that has not been approached by the UAVs on UGV u

until t , a constant is used to mask the value d_t^b in vector \mathbf{x}_t^b ; and for a previously visited stop node b , the newest information d_t^p about the stop node b that approached at t' is used to mask the value d_t^b in vector \mathbf{x}_t^b . The second tensor \mathbf{X}_t^U records the observation of UGVs, denoted as:

$$\mathbf{X}_t^U = [\mathbf{x}_t^1, \dots, \mathbf{x}_t^u, \dots, \mathbf{x}_t^U]^\top, \quad (11a)$$

$$\mathbf{x}_t^u = [x_t^u, y_t^u]^\top, \quad (11b)$$

where \mathbf{x}_t^u denotes the position of a UGV u at t . The observation of a UAV v is then represented by:

$$\mathbf{o}_t^v = \mathbf{s}_t(x_t^v - l : x_t^v + l, y_t^v - l : y_t^v + l), \quad (12)$$

where (x_t^v, y_t^v) is the position of a UAV v , and l is a constant that controls the range of local observation.

The action \mathbf{a}_t^u of a UGV u consists of two parts: $\mathbf{a}_t^u = (\omega, b_{tar})$, where in each timeslot a UGV u first decides whether to release the carried UAVs or not (denoted as ω), and if yes, let b_{tar} be the stop node to reach next. A UAV v 's action $\mathbf{a}_t^v \in \mathbb{R}^2$ specifies its movement behavior in a 2D plane.

The reward function for a UGV u is as follows:

$$r_t^u = \begin{cases} 0, & \omega = \text{False} \\ \sum_{t'=t}^{t+1} (\sum_{v \in \mathcal{V}_u} \Delta d_{t'}^v), & \text{otherwise} \end{cases} \quad (13)$$

If a UGV u decides not to release the carried UAVs and then take further movement to the next stop, it receives zero reward; otherwise, the data collected by the carried UAVs during $[t, t+1]$ will be returned as reward. The reward function for a UAV v is defined as $r_t^v = r_t^{v+} + r_t^{v-}$, where:

$$r_t^{v+} = \text{clip} \left(\frac{\xi_t \Delta d_t^v}{\eta \delta_t^v + \epsilon}, 0, \epsilon_3 \right), \quad (14a)$$

$$\xi_t = \frac{\left(\sum_p (d_0^p - d_t^p) / d_0^p \right)^2}{P \sum_p ((d_0^p - d_t^p) / d_0^p)^2 + \epsilon}. \quad (14b)$$

Here, r_t^{v-} denotes the penalty when a UAV v crashes into obstacles, and ϵ_3, ϵ are both constants. Our goal is to design a MADRL framework that can navigate a group of UGVs and UAVs cooperatively to collect sensory data, while bearing in mind that UAVs and its carrier UGV forms a coalition.

V. PROPOSED SOLUTION: GARN

A. Overview

As shown in Fig. 2, our proposed model GARN mainly consists of a multi-center attention-based GCN ‘MC-GCN’ for UGV specific feature extraction, and a novel GNN-based communication mechanism ‘E-Comm’ for MADRL that allows the UGV cooperations to be adaptive to the constant changing of geometric shapes formed by UGVs. For each UGV $u \in \mathcal{U}$, its structure can be depicted as follows:

$$\tilde{\mathbf{h}}_t^u = \text{MC-GCN}(\mathbf{o}_t^u), \quad (15a)$$

$$\mathbf{h}_t^u = \text{E-Comm}(\tilde{\mathbf{h}}_t^u, \{\tilde{\mathbf{h}}_t^{u'}\}_{u' \in \mathcal{N}(u)}), \quad (15b)$$

$$\pi_{\theta^u}(\mathbf{a}_t^u | \mathbf{h}_t^u) = f_v^\pi(\mathbf{h}_t^u), \quad (15c)$$

$$V_{\theta^u}(\mathbf{h}_t^u) = f_v^V(\mathbf{h}_t^u), \quad (15d)$$

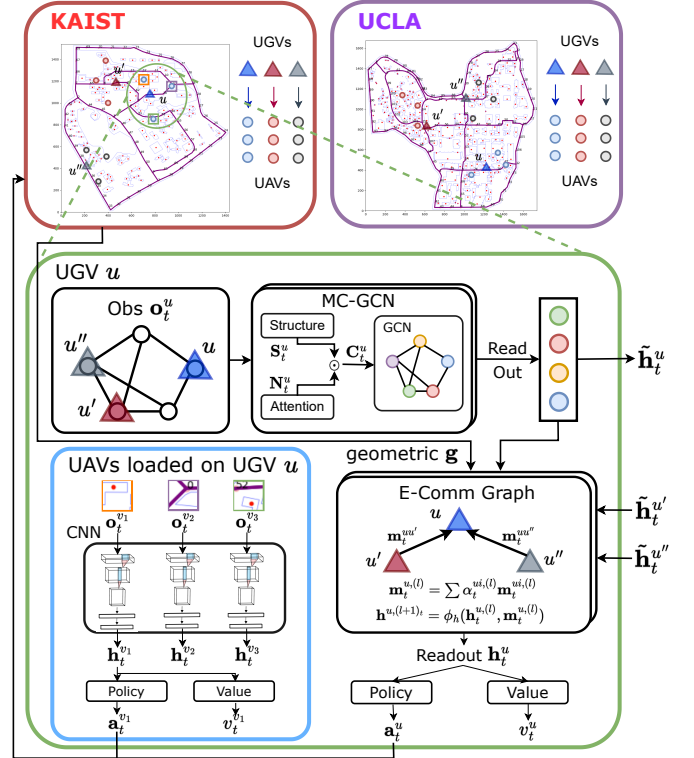


Fig. 2. Overall proposed model GARN.

where $\mathcal{N}(u)$ denotes the set which contains the nearby UGV u' closing to a UGV u ; θ^u contains the total learnable parameters; π_{θ^u} represents policy, and V_{θ^u} represents value function. First, according to Eqn. (15a), MC-GCN takes the current observation \mathbf{o}_t^u of a UGV u as input, and extracts UGV specific features $\tilde{\mathbf{h}}_t^u$ from UGV stop network. Then, E-Comm module combines the UGV specific features and its neighboring UGVs to support geometrically equivalent cooperation and generates compact feature \mathbf{h}_t^u for UGV u (see Eqn. (15b)). Subsequently, through $f_v^\pi(\cdot)$ and $f_v^V(\cdot)$, the compact feature \mathbf{h}_t^u is mapped to an action distribution $\pi_{\theta^u}(\mathbf{a}_t^u | \mathbf{h}_t^u)$ and a value function $V_{\theta^u}(\mathbf{h}_t^u)$, respectively, as shown in Eqn. (15c) and (15d).

Correspondingly, for each UAV $v \in \mathcal{V}$, the whole process can be described as:

$$\mathbf{h}_t^v = \phi_v(\mathbf{o}_t^v), \quad (16a)$$

$$\pi_{\theta^v}(\mathbf{a}_t^v | \mathbf{h}_t^v) = f_v^\pi(\mathbf{h}_t^v), \quad (16b)$$

$$V_{\theta^v}(\mathbf{h}_t^v) = f_v^V(\mathbf{h}_t^v), \quad (16c)$$

where $\phi_v(\cdot)$ contains several CNN layers and outputs a compact feature \mathbf{h}_t^v for UAV v . Then, as shown in Eqn. (16b) and Eqn. (16c), the compact feature is mapped to an action distribution $\pi_{\theta^v}(\mathbf{a}_t^v | \mathbf{h}_t^v)$ and a value function $V_{\theta^v}(\mathbf{h}_t^v)$.

B. UGV Feature Extraction for Spatial Modeling by MC-GCN

In order to make proactive and appropriate decisions for UAVs-UGV coalitions, a UGV is expected to discover useful information from observations for subsequent decision-making. Intuitively, a UGV u has relatively higher possibility

to choose the stop nodes not far away, since a UGV u is more “familiar” to the stop nodes nearby from local observation.

To this end, we propose MC-GCN, a multi-center attention-based GCN to extract UGV specific features from the global stop network. MC-GCN considers not only the position of each UGV itself, but also the positions of its nearby UGVs, to generate more valuable features of stop nodes.

The forward process of MC-GCN can be divided into two phases. First, in Feature Collection Phase, MC-GCN captures two aspects of features (i.e., structure- and node-related features) from the stop network observed by each UGV to obtain graph as intact as possible. Specifically, each UGV maintains its own perceived global stop graph based on their observations, and MC-GCN process is conducted on each graph, respectively. From the perspective of a UGV u , the process of capturing structure-related features can be depicted by:

$$\hat{s}(b_t^u, b) = s(b_t^u, b) - \frac{1}{U-1} \sum_{u' \in \mathcal{U}-\{u\}} s(b_t^{u'}, b), \quad (17a)$$

$$S_t^u = [\hat{s}(b_t^u, 1), \dots, \hat{s}(b_t^u, b), \dots, \hat{s}(b_t^u, B)]^\top, \quad (17b)$$

where $s(\cdot)$ represents a structural correlation function that captures the graphical structural relationship between two nodes (e.g., the reciprocal of shortest path distance), and b_t^u denotes the current stop node of a UGV u at t .

According to Eqn. (17a), $\hat{s}(b_t^u, b)$ can be regarded as structural relevance evaluation of stop node b by UGV u , where the relationship between other UGVs and node b are also taken into account. The structural relevance $s(b_t^{u'}, b)$ of other UGVs on node b is then subtracted to consider the possibility that a stop node b may be accessed by other UGVs. Finally, we combine the structural information from all nodes to get structure-related features S_t^u of a UGV u . Specifically, we introduce shortest path distance [37] between nodes b_m and b_n , as:

$$d_{sp}^q = \begin{cases} d_{sp}(b_m, b_n), & d_{sp}(b_m, b_n) \leq q \\ \infty & \text{otherwise,} \end{cases} \quad (18)$$

where threshold q defines the scope of relevance between nodes. If two nodes whose shortest path distance exceeds q , they are considered as unreachable nodes from each other. MC-GCN uses the reciprocal of the distance, meaning that closer nodes have stronger relationship in graph structure. To avoid the interference of zero denominator, we add a small positive term to the denominator as:

$$s(b_t^u, b) = \frac{1}{d_{sp}^q(b_t^u, b) + 1}. \quad (19)$$

To this end, the structure-related feature S_t^u of UGV u 's observed graph is obtained.

Next, in Feature Extraction Phase, MC-GCN utilizes the previously obtained features to generate the weights of GCN layers, and eventually, obtains the UGV specific feature representation through the GCN with attention module. It guides each UGV to focus more on those stop nodes which not only

have relatively more remaining data (thus collecting them will generate reward), but also far away ones to avoid possible interest overlap. Specifically, the structural-related feature S and node-related feature N are combined to measure the importance of UGV stop nodes by attention mechanism, as:

$$\mathbf{F}_t^{uu', (l)} = \mathbf{H}_t^{u, (l)} \mathbf{W}_1^{(l)} (\mathbf{H}_t^{u, (l)} [b_t^{u'}])^\top, \quad (20a)$$

$$\mathbf{N}_t^{u, (l)} = \mathbf{F}_t^{uu, (l)} - \frac{1}{U-1} \sum_{u' \in \mathcal{U}-\{u\}} \mathbf{F}_t^{uu', (l)}, \quad (20b)$$

$$\mathbf{C}_t^{u, (l)} = \text{Softmax}(\mathbf{S}_t^u \cdot \mathbf{N}_t^{u, (l)}), \quad (20c)$$

where $\mathbf{F}_t^{uu', (l)}$ is the output of attention module in l -th GCN layer with attention reduction and \mathbf{W}_1 is a learnable weight matrix. We use node $b_t^{u'}$ to attend on all other nodes with a UGV in the graph from its perception. Then, similar to structural-related feature, the node-related feature is obtained by subtracting self-node attention from cross-node attention. This kind of operation allows a UGV u to find the important nodes to focus on and keep the interest separated from other UGVs, by considering others' attention on these nodes. Finally, the attention weight \mathbf{C} is combined with these two features by softmax normalization.

The mechanism above is operated in each GCN layer, providing additional weights in the forward process of GCN:

$$\mathbf{H}_t^{u, (l+1)} = \sigma(\mathbf{C}_t^{u, (l)} \cdot (\mathbf{L} \mathbf{H}_t^{u, (l)} \mathbf{W}_2^{(l)})), \quad (21)$$

where \mathbf{L} is the Laplace matrix and $\mathbf{H}_t^{u, (l)}$ is UGV u 's graph input for the l -th layer. For the initial setting, we take $\mathbf{H}_t^{u, (0)} = \hat{\mathbf{X}}_t^{\mathcal{B}, u}$ from a UGV's observation. Finally, the UGV specific features $\tilde{\mathbf{h}}_t^u$ of stop network centered on a UGV u can be extracted from the top layer of GCN outputs:

$$\tilde{\mathbf{h}}_t^u = \phi_H(\mathbf{H}_t^{u, (-1)}), \quad (22)$$

where ϕ_H is a linear readout function.

C. Equivariant Multi-Agent Communication among UGVs by E-Comm

E-Comm is a GNN-based communication mechanism that well adapts to constant changing of geometric shapes formed by UGVs, including transformation and rotation [38]. Existing GNN models are invariant to the change of geometric attributes of graph nodes, which is different from the unevenness of data in our considered air-ground SC task with UAV carriers, that we should carefully consider. As an example, the shape formed by UGVs at a time may keep similar after translation or rotation, but UGVs should behave differently since their geographical positions are changed.

Inspired by Equivariant Graph Neural Networks (EGNNs [39]) which preserved the equivariance of translations, rotations and permutations on a graph, we proposed E-Comm to keep the communication process sensitive to geometric transformation. We regard each UGV as a graph node to build a communication graph, and design the message passing scheme among UGVs, as part of decentralized MADRL. E-Comm consists of invariant *Message Aggregation phase*, and

equivariant *Target Updating phase*, then the composition of them still preserves equivariance. In forward process, we introduce non-geometric feature $h_t^{u,(l)}$ and geometric feature $g_t^{u,(l)}$ into E-Comm layers, which are initialized as:

$$h_t^{u,(0)} = \tilde{h}_t^u, \quad (23a)$$

$$g_t^{u,(0)} = x_t^u. \quad (23b)$$

These two features are messages transmitted among UGVs and updated through E-Comm layers.

1) *Message Aggregation Phase among UGVs*: To aggregate messages from other nodes, E-Comm is operated in a weighted-sum manner, where the weights are designed based on the geometric distance among UGVs. We estimate the distance between UGV u and u' by their geometric feature, as:

$$r_t^{uu',(l)} = g_t^{u,(l)} - g_t^{u',(l)}, u' \in \mathcal{N}(u), \quad (24)$$

where $\mathcal{N}(u)$ represents the neighborhood of a UGV u . Since this subtraction only preserves the relative position between two UGVs, the output is geometrically invariant.

In the communication graph, distant UGVs tend to affect less with each other. For a UGV u , we take reciprocal of the norms $\|r_t^{uu',(l)}\|$ to generate the normalized importance weights $\alpha_t^{uu',(l)}$ of messages from a UGV u' , given $u' \in \mathcal{N}(u)$, as:

$$\alpha_t^{uu',(l)} = \frac{\exp(\|r_t^{uu',(l)}\|^{-1})}{\sum_{u'' \in \mathcal{N}(u)} \exp(\|r_t^{uu'',(l)}\|^{-1})}. \quad (25)$$

With the weights, the message aggregation process in l -th E-Comm layer can be defined by:

$$m_t^{uu',(l)} = \phi_m^{(l)}(h_t^{u',(l)}), \quad (26a)$$

$$m_t^{u,(l)} = \sum_{u' \in \mathcal{N}(u)} \alpha_t^{uu',(l)} m_t^{uu',(l)}, \quad (26b)$$

$$h_t^{u,(l+1)} = \phi_h^{(l)}([h_t^{u,(l)}; m_t^{u,(l)}]), \quad (26c)$$

where ϕ_m and ϕ_h are linear functions. From the view point of a UGV u , the aggregated message $m_t^{u,(l)}$ combines message $m_t^{uu',(l)}$ from other UGVs in its neighborhood. Finally, UGV u 's non-geometric feature is updated by the aggregated message for next layer.

2) *Target Updating Phase among UGVs*: In each E-Comm layer, the geometric feature $g_t^{u,(l)}$ is updated in a radial direction guided by the distance measurement $r_t^{uu',(l)}$ to estimate the target position of a UGV u . It is notable that the measurement $r_t^{uu',(l)}$ contains directional information since this measurement is a subtraction of geometric feature of a pair of UGVs which are learned from coordination in 2D space.

Here, we introduce $\tilde{g}_t^{u,(l)}$ to estimate the joint effect on a UGV u from those UGVs in u 's neighborhood:

$$\tilde{g}_t^{u,(l)} = \sum_{u' \in \mathcal{N}(u)} \alpha_t^{uu',(l)} \phi_g^{(l)}(m_t^{uu',(l)}) \hat{r}_t^{uu',(l)}, \quad (27)$$

where $\phi_g^{(l)}$ is a linear message encoder, $\hat{r}_t^{uu',(l)}$ is the unit vector of $r_t^{uu',(l)}$ to keep directional information only. Referring to resultant force in physics, the vector sum of $\hat{r}_t^{uu',(l)}$ accumulate the effect from others, which tends to keep a UGV u from gathering with other UGVs. Considering this effect, the geometric feature of UGV u is updated by:

$$g_t^{u,(l+1)} = g_t^{u,(l)} + \text{clip}(\tilde{g}_t^{u,(l)}, \tilde{g}_{max}). \quad (28)$$

To constrain the update range, $\tilde{g}_t^{u,(l)}$ is clipped by a constant vector \tilde{g}_{max} .

Finally, we readout the features from the top layer of E-Comm to extract the graph representation. This process is depicted by:

$$z_t^u = \hat{X}_t^{\mathcal{B},u}[:, 2] \mathbf{W}_3(g_t^{u,(-1)})^\top, \quad (29a)$$

$$h_t^u = \phi_u([h_t^{u,(-1)}; z_t^u]), \quad (29b)$$

where z_t^u extracts the relationship between the position of target $g_t^{u,(-1)}$ and all stop nodes, which reflects UGV u 's preference among all stops.

As shown in Eqn. (29b), invariant feature $h_t^{u,(-1)}$ and equivariant feature z_t^u compose the final readout, which is geometrically equivariant as well.

D. Algorithm Description and Computational Complexity Analysis

The entire training process of GARL is shown in Algorithm 1. We train GARL for M iterations.

First, we initialize learnable parameters for UGVs and UAVs, respectively (Line 1), and start the loop for sampling and training (Line 2). Since the base design our model is IPPO, we initialize the training buffer \mathcal{D}^u for a UGV u , and the training buffer \mathcal{D}^v for a UAV v (Line 3). Next, we start the loop for sampling in the air-ground SC environment, where the duration of a task is divided into T timeslots (Line 4). Then, all UGVs interact with the environment together (Line 5). In each timeslot $[t, t+1]$, each UGV u first gets local observation \mathbf{o}_t^u from the environment (Line 6). Then, a UGV u generates its specific feature h_t^u using Eqn. (15a) and Eqn. (15b) (Line 7). After, it samples its own action \mathbf{a}_t^u according to $\pi_{\theta^u}(\mathbf{a}_t^u | h_t^u)$ (Line 8), and calculates value function V_t^u according to $V_{\theta^u}(h_t^u)$ (Line 9). If a UGV u decides to release the loaded UAVs following its sampled action, or a UGV u is still waiting for the UAVs to return, all UAVs released by this UGV will interact with the environment together (Line 10). Each UAV v first gets its local observation \mathbf{o}_t^v from the environment (Line 11). Then, a UAV v extracts its distinct feature h_t^v using Eqn. (16) (Line 12). After, it samples its own action \mathbf{a}_t^v according to $\pi_{\theta^v}(\mathbf{a}_t^v | h_t^v)$ (Line 13), and calculate value function V_t^v according to $V_{\theta^v}(h_t^v)$ (Line 14). After all UGVs and UAVs execute their actions, they will receive an individual reward and the environment transits to next state (Line 15). Then, we start to train the parameters of the neural network models for UGVs and UAVs (Line 16). We compute accumulative rewards $\hat{R}_{1:T}^u$ and advantage $A_{1:T}^u$ from trajectory for each UGV and UAV (Line 17). For a UGV (Line

Algorithm 1: GARN

```

1 Initialize UGV parameter  $\theta^u$  and UAV parameter  $\theta^v$ .
2 for iteration= 1, 2, ⋯, M do
3   Set training buffer  $\mathcal{D}^u = \mathcal{D}^v = \{\}$ ;
4   for  $t = 1, 2, \dots, T$  do
5     for  $u = 1, 2, \dots, U$  do
6       Get local observation  $\mathbf{o}_t^u$ ;
7       Generate feature  $\mathbf{h}_t^u$  by Eqn. (15a) and
8       Eqn. (15b);
9       Sample action  $\mathbf{a}_t^u \sim \pi_{\theta^u}(\mathbf{a}_t^u | \mathbf{h}_t^u)$ ;
10      Calculate value  $V_t^u \leftarrow V_{\theta^u}(\mathbf{h}_t^u)$ ;
11      foreach UAV  $v$  for  $u$  do
12        Get local observation  $\mathbf{o}_t^v$ ;
13        Generate feature  $\mathbf{h}_t^v$  by Eqn. (16);
14        Sample action  $\mathbf{a}_t^v \sim \pi_{\theta^v}(\mathbf{a}_t^v | \mathbf{h}_t^v)$ ;
15        Calculate value  $V_t^v \leftarrow V_{\theta^v}(\mathbf{h}_t^v)$ ;
16      Execute actions of all UGVs and UAVs,
17      receive reward and transit to next state;
18      foreach UGV and UAV do
19        Compute accumulative rewards  $\hat{R}_{1:T}$  and
20        advantage  $A_{1:T}$  from trajectory;
21        if UGV then
22           $\mathcal{D}^u = \mathcal{D}^u \cup \{(\hat{R}_{1:T}, A_{1:T}, V_{1:T})\}$ ;
23        else
24           $\mathcal{D}^v = \mathcal{D}^v \cup \{(\hat{R}_{1:T}, A_{1:T}, V_{1:T})\}$ ;
25      Optimize surrogate loss in Eqn. (3) w.r.t  $\theta^u$  and
26       $\theta^v$ , with  $J$  times and mini-batch sampled from
27       $\mathcal{D}^u$  and  $\mathcal{D}^v$ ;
28       $\theta_{old}^u \leftarrow \theta^u$ ,  $\theta_{old}^v \leftarrow \theta^v$ .

```

18), we add the tuple $(\hat{R}_{1:T}, A_{1:T}, V_{1:T})$ into training buffer \mathcal{D}^u (line 19); otherwise (Line 20), the tuple will be added into training buffer \mathcal{D}^v (Line 21). After collecting the training samples, we start the training process. We optimize θ^u and θ^v by Eqn. (3) in total J times through sampling mini-batches from \mathcal{D}^u and \mathcal{D}^v , respectively (Line 22-23).

GARN includes the vanilla PPO policy network that contains several convolution and linear layers. We compute the time complexity of forward process according to [40]. For UGVs, MC-GCN, E-Comm and PPO network handle vector input, which only contain fully connected layers, as:

$$O\left(\sum_{i=1}^{H_L} D_{1,i} \cdot D_{2,i}\right), \quad (30)$$

where H_L is the number of linear layers; $D_{1,i}$ and $D_{2,i}$ are the dimension of input and output features of i -th linear layers.

For UAVs, they take image input as local observation, thus both convolution layers and linear layers are included in the forward process. The time complexity for UAVs can be

computed by:

$$O\left(\sum_{i=1}^{H_L} D_{1,i} \cdot D_{2,i} + \sum_{i=1}^{H_C} D_{3,i}^2 \cdot D_{4,i}^2 \cdot D_{5,i} \cdot D_{6,i}\right), \quad (31)$$

where H_L and H_C is the number of linear layers and convolution layers; $D_{1,i}$ and $D_{2,i}$ are the dimension of input and output features of i -th linear layers; $D_{3,i}$, $D_{4,i}$, $D_{5,i}$ and $D_{6,i}$ are the size of output feature maps and convolution kernel, the number of input channels and output channels of the i -th convolution layer.

VI. PERFORMANCE EVALUATION

A. Campus Description and Simulation Setting

We use two campuses KAIST, South Korea and UCLA, USA, to simulate our considered air-ground SC task with UAV carriers, and in particular to collect CCTV camera and sensory data deployed in/around the buildings. Campus landscape data are obtained from Google Map by using OpenStreetMap and pre-processed for our simulation, including setting the boundaries of buildings and the trace of roads. KAIST campus has a relatively simpler road network, while UCLA campus is more complicated. Google Map is used to mark the positions and the shapes of buildings and mountains. KAIST spans 1433.37 meters from north to south and 1539.63 meters from east to west, covering about 2.21 million square meters. We randomly placed 138 sensors on 85 buildings; UCLA spans 1737.15 from north to south and 1675.36 from east to west, covering 2.91 million square meters. Likewise, we place 236 sensors on 163 buildings in UCLA campus.

UAVs have weak long-distance travelling capability due to limited battery supply but good short-distance mobility. However, UGVs have good long-distance mobility but can only move following the roads. We set the length of each timeslot as 30 seconds. Each sensor p is initialized with data amount d_0^p , which is randomly generated within range 1GB to 1.5GB. The initial location of each UGV is set in the center of two campuses. According to TS-X4, the maximum flying speed of UAVs is 12km/h and its initial energy reserve is $e_0 = 10\text{kJ}$ [41]. Energy consumption weight factor $\eta = 0.01\text{kJ/m}$, the sensing range for UAVs is 60 meters, and the data collection rate for UAVs are 166.7 Mbps per sensor, respectively. For UGVs, we put UGV stops every 100 meters along the roads and assume that UGVs can maximally travel 400 meters in a timeslot (equivalent to the maximum speed 48km/h [42]).

In all the experiments, we use Pytorch 1.8.1 to implement our proposed model, and all the codes are run on Ubuntu 18.04.2 LTS with 8 GeForce RTX A6000 graphic cards. We conduct three sets of experiments, including impact of hyperparameters, ablation study and comparing with baselines. Results are compared from data collection ratio ψ , fairness ξ , cooperation factor ζ and low energy consumption ratio β , as well as the final performance index efficiency λ .

TABLE II
IMPACT OF NO. OF LAYERS IN MC-GCN L^{MC} AND NO. OF LAYERS IN E-COMM L^E (WHEN $U = 4, V' = 2$).

Campus	Metric	L^{MC}					L^E				
		1	2	3	4	5	1	2	3	4	5
KAIST	λ	0.8280	0.9211	0.9970	0.9760	0.8665	0.7215	0.9064	0.9970	0.9852	0.9487
	ψ	0.5023	0.4221	0.6198	0.5234	0.5236	0.5394	0.5552	0.6198	0.6156	0.5937
	ξ	0.5282	0.4439	0.6391	0.5513	0.5475	0.5558	0.5716	0.6391	0.6323	0.6209
	ζ	0.7025	0.7676	0.6760	0.7277	0.6588	0.5445	0.5174	0.6760	0.5783	0.6270
	β	0.2361	0.1663	0.2786	0.2228	0.2255	0.2533	0.1913	0.2786	0.2493	0.2539
UCLA	λ	0.5190	0.5619	0.6137	0.5961	0.5658	0.5099	0.5548	0.6137	0.5804	0.5645
	ψ	0.3600	0.3634	0.4511	0.3897	0.3891	0.3510	0.3716	0.4511	0.3730	0.3725
	ξ	0.3812	0.3818	0.4667	0.4121	0.4155	0.3723	0.3885	0.4667	0.3981	0.3951
	ζ	0.7230	0.7346	0.7244	0.7215	0.7435	0.7005	0.6913	0.7244	0.7703	0.7422
	β	0.1985	0.1882	0.2613	0.2024	0.2193	0.1939	0.2000	0.2613	0.2109	0.2059

TABLE III
ABLATION STUDY ($U = 4$ AND $V' = 2$).

Campus	Method	λ	ψ	ξ	ζ	β
KAIST	GARL	0.9970	0.6198	0.6391	0.6760	0.2786
	GARL w/o MC	0.7036	0.4952	0.5205	0.6575	0.2530
	GARL w/o E	0.8119	0.5303	0.5548	0.6760	0.2573
	GARL w/o MC, E	0.5810	0.4478	0.4742	0.6269	0.2470
UCLA	GARL	0.6137	0.4511	0.4667	0.7244	0.2613
	GARL w/o MC	0.4114	0.3553	0.3799	0.7039	0.2426
	GARL w/o E	0.5080	0.3721	0.3898	0.7163	0.2123
	GARL w/o MC, E	0.3396	0.3200	0.3343	0.7033	0.2356

B. Impact of Hyperparameters

We select two key hyperparameters from MC-GCN, where L^{MC}, L^E determines the number of layers in MC-GCN, E-Comm, respectively. As shown in Table II, we find that all of two hyperparameters yield a peak value in terms of efficiency. When L^{MC} is too small, the receptive field of each UGV stop node during graph convolution will not be big enough to consider sufficient neighboring nodes' features; in another extremity, when the L^{MC} is too big, the features extracted from each UGV stop node are too general since they consider too many nodes which are far away. Obviously, either extremity worsens the overall performance. Similarly, in E-Comm, when the L^E is too small, each UGV can only obtain the information of UGVs nearby, which will result in low level of cooperative policies for the UAVs-UGV coalition. On the other hand, when the L^E is too big, the received message may contain redundant information which makes it difficult for a UGV to extract useful ones from the message. Therefore, we choose $L^{MC} = 3$ and $L^E = 3$ as the best hyperparameters used in the following experiments.

C. Ablation Study

We choose 4 UGVs and 2 UAVs per UGV as the setting of our ablation study, which is performed by gradually removing two key components of our model, i.e., MC-GCN (MC) and E-Comm (E). As shown in Table III, the complete model GARL achieves 41.70% and 49.17% higher efficiency than that of GARL w/o MC in KAIST and UCLA campuses, respectively. This confirms that proposed MC-GCN model is able to extract feature from the state more comprehensively especially when the environment (i.e., UCLA campus) is more complicated (compared to KAIST campus). If not,

GCN employs only graph convolution, missing the different importance between neighboring nodes generated by attention mechanism as in our proposed MC-GCN. Thus the feature extraction may attach more importance on nodes far away, which will lead the UGVs to go to certain places with less data to collect. GARL achieves 22.81% and 20.79% higher efficiency than that of GARL w/o E in two campuses, due to the help of our proposed communication mechanism between UGVs in message integration. This benefit is clear for UCLA campus whose topographic landscape is more irregular and its east/west parts are connected with a thin area which does not contain much data to be collected. Furthermore, GARL w/o MC achieves 21.09% and 21.16% higher efficiency than that of GARL w/o MC, E in two campuses. Finally, GARL w/o E achieves 39.72% and 49.61% higher efficiency than that of GARL w/o MC, E in two campuses, which proves that our proposed MC-GCN model do help UGVs accurately locate the most important information relevant to the current UGV's partial observation.

D. Comparing with Eight Baselines

We compare our method GARL with eight baselines, as:

- **CubicMap** [21]: It is a memory augmented CNN-based method with cubic writing and spatially contextual reading mechanisms to extract long-term spatiotemporal features. We consider it as the state-of-the-art approach for UAV-aided SC.
- **GAM** [9]: It is a GNN based method that adaptively accesses the sequence of UGV stop nodes ordered by the importance to extract both long-term and short-term spatiotemporal features. We consider it as the state-of-the-art approach for spatial modeling.
- **GAT** [8]: It is a classical graph feature extraction method as an extension of GNN where attention mechanism is used to attach importance on different neighboring nodes.
- **AE-Comm** [43]: It designs a communication auto-encoder to generate a common language among all MADRL agents. This auto-encoder is used to transform the agent's observation to the common language representation. We consider it as the state-of-the-art approach for communication based MADRL methods.

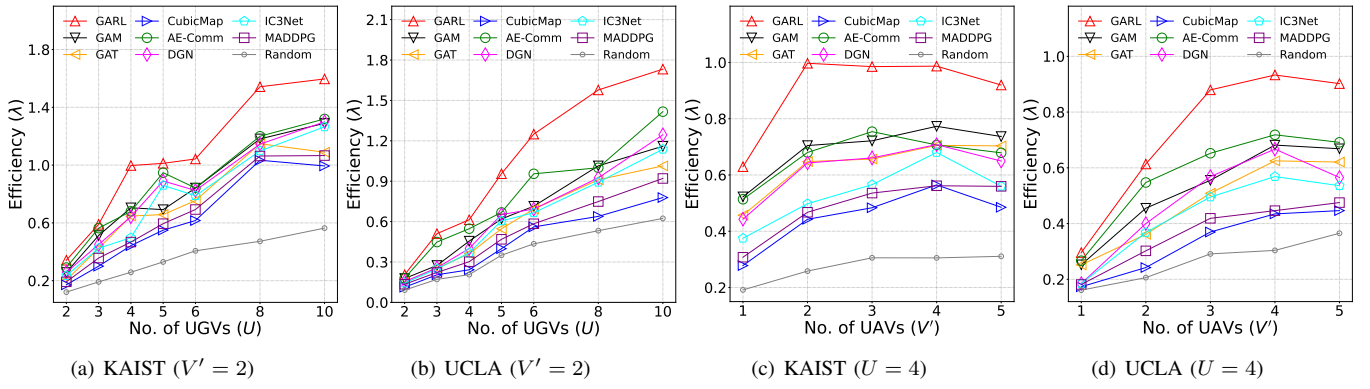


Fig. 3. Impact of no. of UGVs and UAVs in terms of efficiency λ .

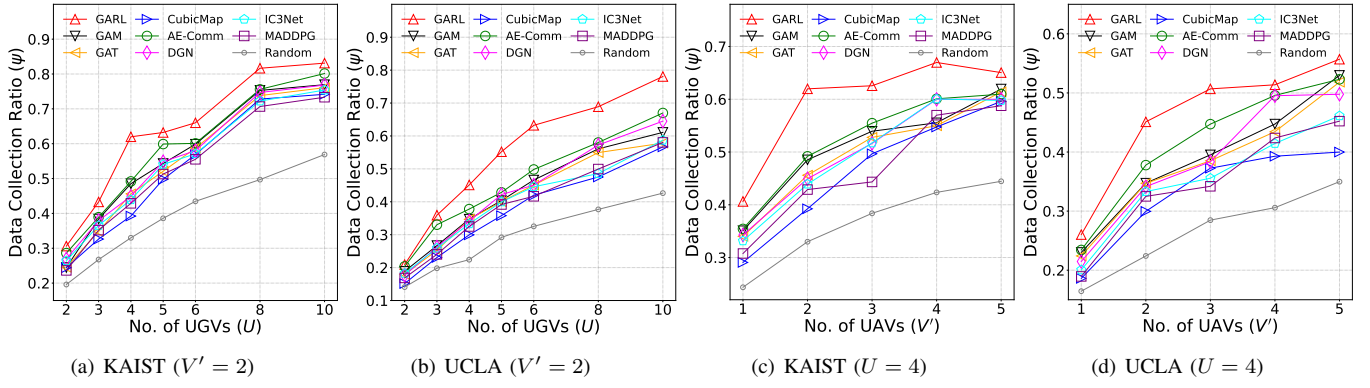


Fig. 4. Impact of no. of UGVs and UAVs in terms of data collection ratio ψ .

- **DGN** [44]: It is an attention based method to enhance agent communication that attaches different importance on neighboring nodes and aggregates their messages according to their importance.
- **IC3Net** [10]: It is a classical communication model for multi-agent environment which uses individualized LSTM policy and a gating mechanism to control when to communicate among agents.
- **MADDPG** [30]: It is a classical MADRL method aided by a distributed prioritized experience replay.
- **Random**: For each UGV and UAV, we sample an action uniformly from action space.

Results are shown in Fig. 3 - Fig. 6. We make four important observations.

Our proposed model GARN consistently outperforms all eight baselines in terms of efficiency in both KAIST and UCLA campus environments. The reason comes from three aspects, namely: accurate feature extraction from spatial modeling, efficient communication mechanism among UAGs, and used underlying MADRL base model. In terms of spatial modeling, CubicMap is a memory augmented CNN-based method, but not based on GNN, thus cannot have clear overview of the geometric structure of the UGV stop network, which is crucial in our considered air-ground SC tasks with UAV carriers. GAT uses attention mechanism to capture the different degrees of importance of immediate neighboring UGV stop nodes, however it does not consider all other UGV

stop nodes which can be a bit far away but still useful to understand the current entire workzone state. GAM slightly outperforms GAT, due to its combination with GNN and LSTM that traverses all the neighboring stop nodes. Since both methods are built on the view of single UGV, they can not distinguish the benefits brought by other UGVs, thus it is likely that UGVs may gather together around certain stop nodes with high importance without exploring the whole workzone, resulting in poor fairness, data collection ratio, and ultimately overall efficiency.

In terms of communication mechanism among MADRL agents, IC3Net employs LSTM to aggregate the messages received from other UGVs during several past timeslots. This helps learn from historical actions, however simply using average operation to compute target estimation is not enough which blurs the distinct geometric feature of neighboring UGVs. For example, UCLA campus is more irregular compared with KAIST, thus IC3Net performs much worse than other baselines in UCLA. DGN uses attention mechanism to evaluate the importance of messages from neighboring UGVs. However, it does not fully consider the constant geometrical changes of the shape formed by UGVs into the design of MADRL communication mechanism, which is quite essential especially when sensory data distribution is not uniform. AE-Comm outperforms DGN and IC3Net by a large margin, due to its employed auto-encoder scheme that generates a common language among all agents. It transforms local ge-

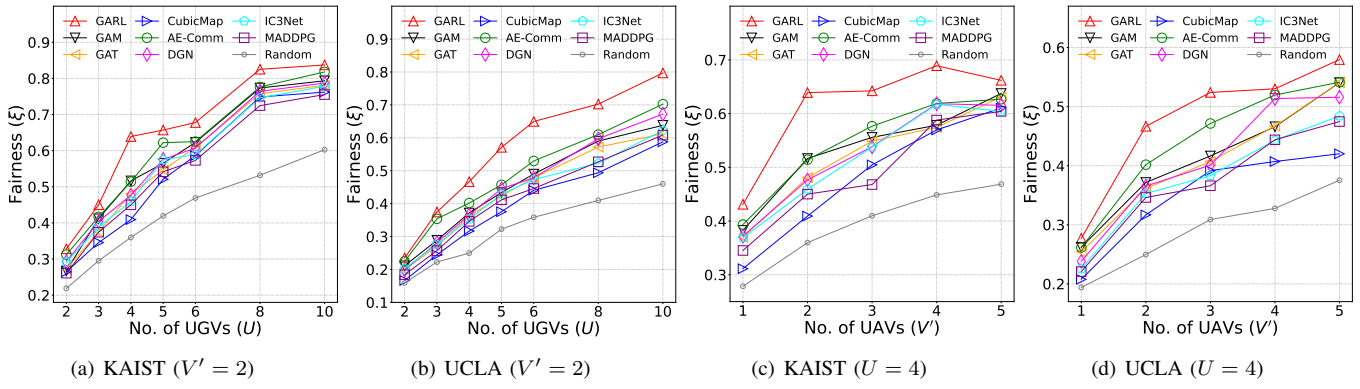


Fig. 5. Impact of no. of UGVs and UAVs in terms of fairness ξ .

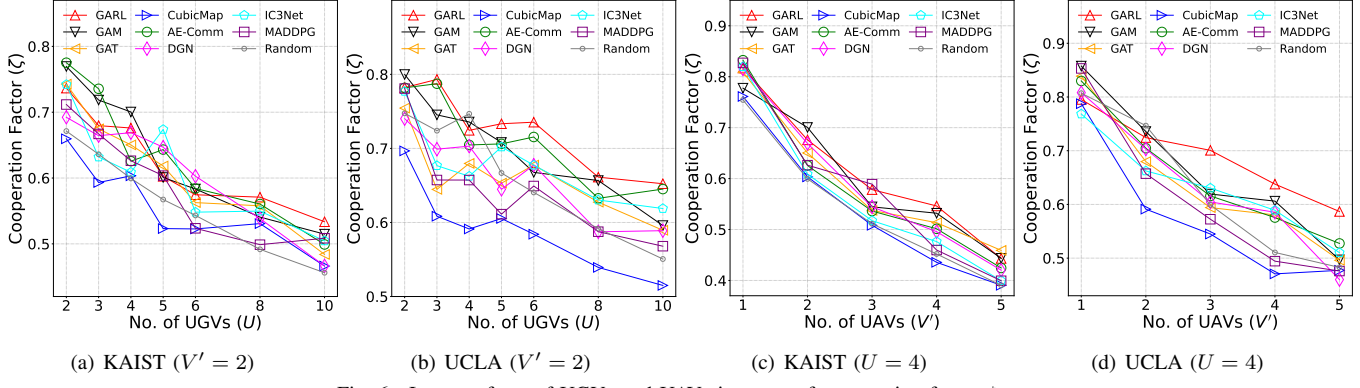


Fig. 6. Impact of no. of UGVs and UAVs in terms of cooperation factor ζ .

ometric feature into a global language for all the UGVs to understand, so the message aggregation phase will be much easier and comprehensive. As a result, the extracted feature from messages is clearer, and making the policy model and value critic model more accurate. Unfortunately, AE-Comm lacks a mechanism to carefully handle the spatial information; as a result, its performance is worse than our methods.

In terms of used underlying MADRL base model, although MADDPG is quite classical, its employed deterministic policy DDPG is not good at action exploration, which is crucial in our campus environment. We use IPPO as the start point of our design, which has much better capability to explore the complex environment than MADDPG.

The spatial complexity of two campus environments has big impact on the performance of all methods. In GARN, we see that UCLA cannot obtain the same level of efficiency as KAIST, when fewer UGVs and UAVs are employed. However, as more UGVs are added (thus loaded UAVs as coalitions), UCLA receives much higher efficiency than KAIST. This is because that not much data can be found in the center of UCLA campus (fewer building as lawns), and in order to collect data in the west, UAVs need to be carried by UGVs, possibly from east to the west. This observation is consistent for other spatial modeling baselines, that performance under KAIST is better than UCLA.

When increasing the number of UGVs, the efficiency, fairness and data collection ratio of all methods go up. For

example, when U changes from 6 to 8, efficiency is increased by 47.92% in KAIST and 26.26% in UCLA (see Fig. 3(a) and Fig. 3(b)). This is because 6 UGVs cannot collect all the data from nearby area so that UGVs will not send UAVs to farther places to collect data. On the other hand, when 8 UGVs well cooperate with each other, data nearby is completely collected so our method allows UGVs to carry their loaded UAVs to reach far away areas. However, cooperation factor of our method goes up first and then down in KAIST, while going straight down in UCLA (see Fig. 6(a) and Fig. 6(b)). We hypothesize that at first, more UGVs will help enhance the performance of UGV-UAVs coalition, but too many UGVs will not bring further benefits. This is because the loaded UAVs may compete with each other to collect sensory data leading to the decrease of data collection ratio.

When increasing the number of UAVs loaded on each UGV, Random approach does not change much for all metrics because it lacks enough explorations or spatial modeling. The attained efficiency from other methods first goes up then down, as shown in Fig. 3(c) and Fig. 3(d) in KAIST. This is because that there may not be enough data to collect around a single UGV thus UAVs released by this UGV will waste time searching in the same area. As a result, we see data collection ratio goes up but both fairness and cooperation factor go down. In UCLA, efficiency will go up rapidly from $V' = 1$ to $V' = 4$ (see in Fig. 3(d)), and then fall down when $V' = 5$, so the bottleneck becomes the number of UGV-UAVs

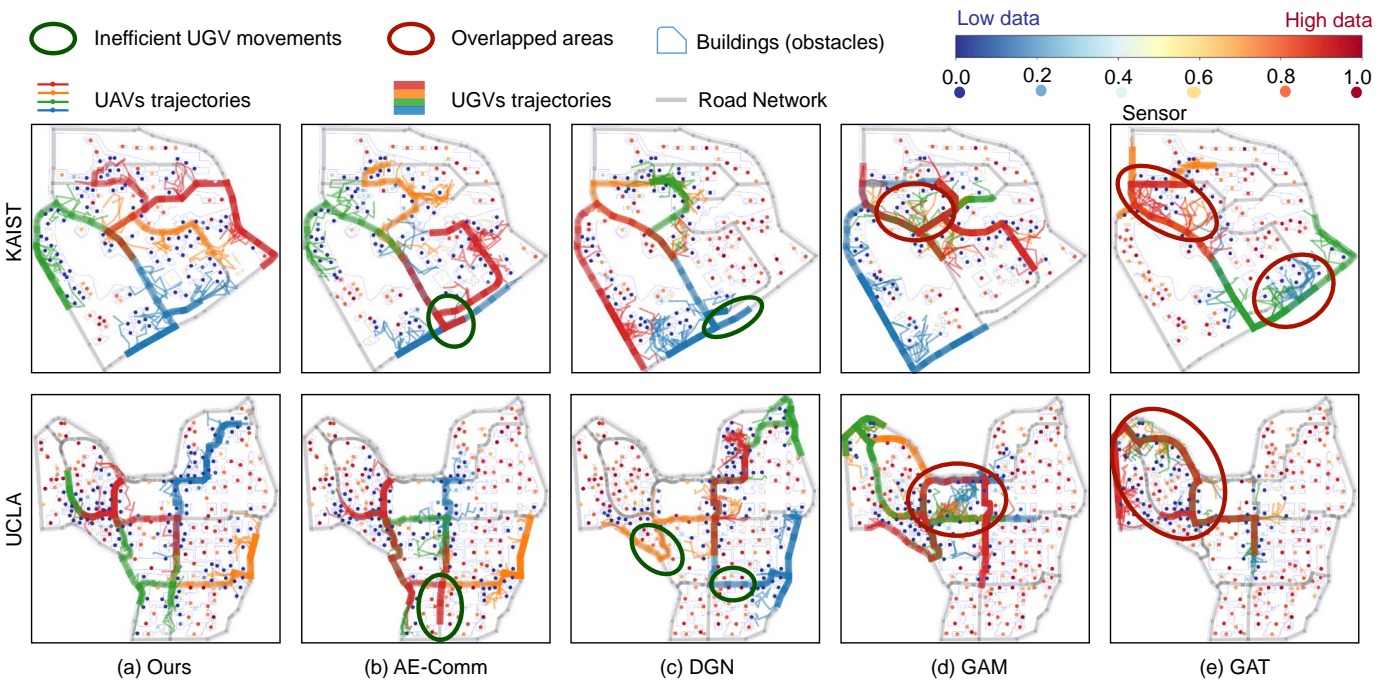


Fig. 7. Movement trace of UGVs and UAVs in KAIST and UCLA (when $U = 4$ and $V' = 2$).

coalition for range extension. In terms of cooperation factor, all methods give downward trend (see Fig. 6(c) and Fig. 6(d)). This is because that since all the UAVs in a particular UGV are released at the same point, competition is inevitable, leaving an insight that too many UAVs on one single UGV may not be helpful to bring further benefits.

E. Illustrative Trajectories of UGV-UAVs Coalitions

In Fig. 7, we show the trace of UGV-UAVs coalitions after running 100 timeslots when $U = 4$, $V' = 2$. We choose four best baselines (two communication based methods and two spatial modeling methods), AE-Comm, DGN, GAM and GAT, for illustration, according to Section VI-D, as well as GARL. We see that AE-Comm and DGN lead to meaningless UGV wanderings in the same areas multiple times (see inefficient UGV movement in KAIST, from Fig. 7(b) and Fig. 7(c)), or simply carrying UAVs to move around even if there is adequate data to be collected (see inefficient UGV movement in UCLA, from Fig. 7(b) and Fig. 7(c)). However, this phenomenon is not likely to happen in GAM or GAT, but may lead to competitive UGV gathering in the same area (see overlapped areas in Fig. 7(d) and Fig. 7(e)). On the contrary, our method GARL produces nice UGV trajectories to be responsible for a sub-workzone (no overlapping or missing data movements), to release the UAVs to collect the data nearby, before heading to the next UGV stop.

F. Computational Complexity Analysis

Computational complexity in terms of both time cost and graphic card memory usage during testing phase is shown in Table IV. With $U = 4$ and $V' = 2$, we observe the running time for a UGV from inputting observation to producing actions in a timeslot by our method GARL. The time cost

TABLE IV
COMPUTATIONAL COMPLEXITY OF ALL METHODS.

Method	Time Cost (ms)		Graphic Card Mem. Usage (MB)	
	KAIST	UCLA	KAIST	UCLA
GARL	0.553	1.121	935	937
GAM [9]	0.66	1.167	939	945
GAT [8]	0.493	0.552	813	841
CubicMap [21]	1.023	2.417	1348	1506
AE-Comm [43]	0.552	0.786	907	943
DGN [44]	0.379	0.523	935	937
IC3Net [10]	0.688	0.892	975	997
MADDPG [30]	2.108	3.892	805	836

is slightly higher than some baselines. However, it is still in the scale of millisecond, which is negligible in practice. Even if our proposed model GARL uses relatively high amount of graphic card memory compared with MADDPG, it is still acceptable compared with the benefits it brings, which has been shown in previous sections.

VII. CONCLUSION

In this paper, we explicitly consider a new type of air-ground SC tasks with UAV carriers, and navigate a group of UGV-UAVs coalitions to perform sensory data collection. Specifically, we propose a novel deep model called GARL, which consists of a spatial modeling module MC-GCN (to extract UGV specific feature from its own observation of UGV stop network), and E-Comm for MADRL communication (equivariant to geometric transformation of the shape formed by UGVs considering uneven distribution of data over the environment). We conduct extensive experiments on two campus environments KAIST and UCLA, where results confirm that our proposed method consistently outperforms all eight baselines in terms of efficiency.

REFERENCES

[1] Z. Chen, P. Cheng, Y. Zeng, and L. Chen, "Minimizing maximum delay of task assignment in spatial crowdsourcing," in *IEEE ICDE'19*, 2019, pp. 1454–1465.

[2] Y. Cheng, B. Li, X. Zhou, Y. Yuan, G. Wang, and L. Chen, "Real-time cross online matching in spatial crowdsourcing," in *IEEE ICDE'20*, 2020, pp. 1–12.

[3] C. H. Liu, Y. Zhao, Z. Dai, Y. Yuan, G. Wang, D. Wu, and K. K. Leung, "Curiosity-driven energy-efficient worker scheduling in vehicular crowdsourcing: A deep reinforcement learning approach," in *IEEE ICDE'20*, 2020, pp. 25–36.

[4] Z. Chen, P. Cheng, L. Chen, X. Lin, and C. Shahabi, "Fair task assignment in spatial crowdsourcing," *Proc. VLDB Endow.*, vol. 13, no. 11, pp. 2479–2492, 2020. [Online]. Available: <http://www.vldb.org/pvldb/vol13/p2479-chen.pdf>

[5] M. Samir, S. Sharafeddine, C. M. Assi, T. M. Nguyen, and A. Ghayeb, "Uav trajectory planning for data collection from time-constrained iot devices," *IEEE Transactions on Wireless Communications*, vol. 19, no. 1, pp. 34–46, 2020.

[6] J. Li, H. Zhao, H. Wang, F. Gu, J. Wei, H. Yin, and B. Ren, "Joint optimization on trajectory, altitude, velocity, and link scheduling for minimum mission time in uav-aided data collection," *IEEE Internet of Things Journal*, vol. 7, no. 2, pp. 1464–1475, 2020.

[7] T. Kipf and M. Welling, "Semi-supervised classification with graph convolutional networks," *ArXiv*, vol. abs/1609.02907, 2017.

[8] P. Veličković, G. Cucurull, A. Casanova, A. Romero, P. Lio, and Y. Bengio, "Graph attention networks," *arXiv preprint arXiv:1710.10903*, 2017.

[9] A. Wijesinghe and Q. Wang, "A new perspective on" how graph neural networks go beyond weisfeiler-lehman?", in *ICLR'21*, 2021.

[10] A. Singh, T. Jain, and S. Sukhbaatar, "Learning when to communicate at scale in multiagent cooperative and competitive tasks," in *ICLR'18*, 2018.

[11] S. Sukhbaatar, R. Fergus *et al.*, "Learning multiagent communication with backpropagation," *NIPS'16*, vol. 29, 2016.

[12] Y. Wang, J. Xu, Y. Wang *et al.*, "Tom2c: Target-oriented multi-agent communication and cooperation with theory of mind," in *ICML'21*, 2021.

[13] C. S. de Witt, T. Gupta, D. Makoviichuk, V. Makoviichuk, P. H. Torr, M. Sun, and S. Whiteson, "Is independent learning all you need in the starcraft multi-agent challenge?" *arXiv preprint arXiv:2011.09533*, 2020.

[14] L. Kazemi and C. Shahabi, "Geocrowd: enabling query answering with spatial crowdsourcing," in *Proceedings of the 20th international conference on advances in geographic information systems*, 2012, pp. 189–198.

[15] W. Ni, P. Cheng, L. Chen, and X. Lin, "Task allocation in dependency-aware spatial crowdsourcing," in *IEEE ICDE'20*, 2020, pp. 985–996.

[16] P. Cheng, L. Chen, and J. Ye, "Cooperation-aware task assignment in spatial crowdsourcing," in *IEEE ICDE'19*, 2019, pp. 1442–1453.

[17] Y. Zhao, K. Zheng, Y. Cui, H. Su, F. Zhu, and X. Zhou, "Predictive task assignment in spatial crowdsourcing: a data-driven approach," in *IEEE ICDE'20*, 2020, pp. 13–24.

[18] H. To, C. Shahabi, and L. Xiong, "Privacy-preserving online task assignment in spatial crowdsourcing with untrusted server," in *IEEE ICDE'18*, 2018, pp. 833–844.

[19] Z. Zhou, J. Feng, B. Gu, B. Ai, S. Mumtaz, J. Rodriguez, and M. Guizani, "When mobile crowd sensing meets UAV: energy-efficient task assignment and route planning," *IEEE Trans. Commun.*, vol. 66, no. 11, pp. 5526–5538, 2018. [Online]. Available: <https://doi.org/10.1109/TCOMM.2018.2857461>

[20] C. H. Liu, X. Ma, X. Gao, and J. Tang, "Distributed energy-efficient multi-uav navigation for long-term communication coverage by deep reinforcement learning," *IEEE Transactions on Mobile Computing*, vol. 19, no. 6, pp. 1274–1285, 2020.

[21] Y. Wang, C. H. Liu, C. Piao, Y. Yuan, R. Han, G. Wang, and J. Tang, "Human-drone collaborative spatial crowdsourcing by memory-augmented and distributed multi-agent deep reinforcement learning," in *IEEE ICDE'22*, 2022, pp. 459–471.

[22] J. Zhang, Z. Yu, S. Mao, S. C. G. Periaswamy, J. Patton, and X. Xia, "Iadrl: Imitation augmented deep reinforcement learning enabled ugv-uav coalition for tasking in complex environments," *IEEE Access*, vol. 8, pp. 102 335–102 347, 2020.

[23] M. Schlichtkrull, T. N. Kipf, P. Bloem, R. v. d. Berg, I. Titov, and M. Welling, "Modeling relational data with graph convolutional networks," in *European semantic web conference*. Springer, 2018, pp. 593–607.

[24] R. Li, S. Wang, F. Zhu, and J. Huang, "Adaptive graph convolutional neural networks," in *AAAI'18*, vol. 32, no. 1, 2018.

[25] L. Wu, P. Sun, R. Hong, Y. Fu, X. Wang, and M. Wang, "Socialgcn: An efficient graph convolutional network based model for social recommendation," *arXiv preprint arXiv:1811.02815*, 2018.

[26] M. Sakai, K. Nagayasu, N. Shibui, C. Andoh, K. Takayama, H. Shirakawa, and S. Kaneko, "Prediction of pharmacological activities from chemical structures with graph convolutional neural networks," *Scientific reports*, vol. 11, no. 1, pp. 1–14, 2021.

[27] L. Bai, L. Yao, C. Li, X. Wang, and C. Wang, "Adaptive graph convolutional recurrent network for traffic forecasting," *NeurIPS'20*, vol. 33, pp. 17804–17815, 2020.

[28] J. Gilmer, S. S. Schoenholz, P. F. Riley, O. Vinyals, and G. E. Dahl, "Neural message passing for quantum chemistry," in *ICML'17*, 2017, pp. 1263–1272.

[29] F. A. Oliehoek and C. Amato, *A concise introduction to decentralized POMDPs*. Springer, 2016.

[30] R. Lowe, Y. I. Wu, A. Tamar, J. Harb, O. Pieter Abbeel, and I. Mordatch, "Multi-agent actor-critic for mixed cooperative-competitive environments," *NIPS'17*, vol. 30, 2017.

[31] J. Foerster, G. Farquhar, T. Afouras, N. Nardelli, and S. Whiteson, "Counterfactual multi-agent policy gradients," in *AAAI'18*, vol. 32, no. 1, 2018.

[32] T. Rashid, M. Samvelyan, C. Schroeder, G. Farquhar, J. Foerster, and S. Whiteson, "Qmix: Monotonic value function factorisation for deep multi-agent reinforcement learning," in *ICML'18*, 2018, pp. 4295–4304.

[33] A. Das, T. Gervet, J. Romoff, D. Batra, D. Parikh, M. Rabbat, and J. Pineau, "Tarmac: Targeted multi-agent communication," in *ICML'19*, 2019, pp. 1538–1546.

[34] C. Yu, A. Veliu, E. Vinitsky, Y. Wang, A. Bayen, and Y. Wu, "The surprising effectiveness of ppo in cooperative, multi-agent games," *arXiv preprint arXiv:2103.01955*, 2021.

[35] J. Schulman, P. Moritz, S. Levine, M. Jordan, and P. Abbeel, "High-dimensional continuous control using generalized advantage estimation," *arXiv preprint arXiv:1506.02438*, 2015.

[36] R. K. Jain, D.-M. W. Chiu, W. R. Hawe *et al.*, "A quantitative measure of fairness and discrimination," *Eastern Research Laboratory, Digital Equipment Corporation, Hudson, MA*, 1984.

[37] A. Madkour, W. G. Aref, F. U. Rehman, M. A. Rahman, and S. Basalamah, "A survey of shortest-path algorithms," *arXiv preprint arXiv:1705.02044*, 2017.

[38] J. Han, Y. Rong, T. Xu, and W. Huang, "Geometrically equivariant graph neural networks: A survey," *arXiv preprint arXiv:2202.07230*, 2022.

[39] V. G. Satorras, E. Hoogeboom, and M. Welling, "E (n) equivariant graph neural networks," in *ICML'21*, 2021, pp. 9323–9332.

[40] K. He and J. Sun, "Convolutional neural networks at constrained time cost," in *IEEE CVPR'15*, 2015, pp. 5353–5360.

[41] "TS-X4," <http://www.droneeye.com/droneDetail/138>.

[42] "D80," <https://auto.dji.com/cn/solution-d80>.

[43] T. Lin, J. Huh, C. Stauffer, S. N. Lim, and P. Isola, "Learning to ground multi-agent communication with autoencoders," *NeurIPS'21*, vol. 34, pp. 15 230–15 242, 2021.

[44] J. Jiang, C. Dun, T. Huang, and Z. Lu, "Graph convolutional reinforcement learning," in *ICLR'19*, 2019.